Acta Mechanica 113, 119–135 (1995)

ACTA MECHANICA

Stress concentration at irregular surfaces of anisotropic half-spaces

E. Pan and **B. Amadei,** Boulder, Colorado

(Received December 8, 1993; revised May 10, 1994)

Summary. An analytical method is presented to derive the stresses in anisotropic half-spaces with smooth and irregular surface morphologies. The half spaces can be subjected to body forces, surface tractions, and uniform far-field stresses. The general solution is expressed in terms of three analytical functions using the analytical function method of anisotropic elasticity. These three functions are then determined using a numerical conformal mapping technique and an integral equation method. Numerical examples are presented for the stress concentration at irregular surfaces induced by a uniform far-field horizontal stress. The elastic half-spaces are assumed to be transversely isotropic or isotropic, and their surface morphologies are constructed by the superposition of multiple long and symmetric ridges (mounds) and valleys (depressions). For isotropic media, the stress concentration depends only on the half-space surface geometry. It is found here that for anisotropic media, the half-space surface geometry, as well as the orientation of the planes of material anisotropy, have a great effect on the stress concentration. The degree of material anisotropy, on the other hand, has little influence on the stress concentration.

1 Introduction

Stress concentration at the irregular surface of a half space has been addressed in the past using three types of analytical methods. One is the bipolar coordinate transform method as discussed by Ling [1] for circular notches. Another is the exact conformal mapping method, as studied by Savage and Swolfs [2] for long symmetric ridges and valleys, and recently by Chiu and Gao [3] for a cycloid rough surface. However, these two methods are restricted to isotropic media and to simple surface profiles. The third approach is the perturbation method discussed by Srolovitz [4] and Gao [5], [6], which can only be used for surface profiles with small amplitudes.

In a recent paper, Pan and Amadei [7] presented a new analytical method for determining the stress field in a homogeneous, general anisotropic and elastic half space subject to gravity and surface loads under a condition of generalized plane strain and limited by irregular (but smooth) outer boundaries. Using the closed-form solutions of Amadei and Pan [8] and the analytical function method of Lekhnitskii [9], expressions for the stresses in an anisotropic half space with an irregular outer boundary were derived. The stresses were found to depend on three analytical functions that can be determined using a numerical conformal mapping method [10] and an integral equation method [11]. This solution has been extended more recently by the authors [12] to determine tectonic as well as gravitational stresses in irregular half-spaces.

In this paper, we first derive an analytical solution for the stress field caused by the combined effect of body forces, surface tractions, and uniform far-field stresses in anisotropic half-spaces with irregular surfaces. This is an extension of the authors' previous solutions [7], [12] to the general case of body forces and far-field stresses. In order to illustrate the present solution, numerical examples are presented to show how various parameters affect the stress concentra-

tion at irregular surfaces induced by a uniform far-field horizontal stress. The elastic half-spaces are assumed to be transversely isotropic or isotropic. It is found that the stress concentration depends greatly on the half-space's surface geometry and the orientation of the planes of material anisotropy, and to a lesser extent on the degree of material anisotropy.

2 Basic equations

Consider the equilibrium of a half space with the geometry of Fig. 1. The medium in the half space is assumed to be linearly elastic, homogeneous, anisotropic and continuous with a uniform density ϱ. An x, y, z coordinate system is attached to the half space such that the x and z axes are in the horizontal plane and the y axis is pointing upward. The half space is subject to surface tractions t_i $(i = x, y, z)$, body forces F_i $(i = x, y, z)$, and a uniform far-field stress field σ_{ij}^0 $(i, j = x, y, z)$. We assume that the geometry, the elastic properties of the medium, the surface tractions and body forces are independent of the z direction. We also assume that the boundary curve of the half space can be described by an analytic function $y = y(x)$ or in parametric form $x = x(t)$, $y = y(t)$.

The problem is to find the magnitude and distribution of the stresses induced by the surface tractions, body forces and/or the far-field stresses in the half space. Since the geometry of the problem is independent of the z coordinate and the medium is homogeneous, the stresses can be determined assuming a condition of generalized plane strain, e.g. all planes normal to the z axis are assumed to warp identically [9]. In general, the stresses and strains must satisfy the following equations:

2.1 *Equations of equilibrium*

$$\begin{aligned} \frac{\partial \sigma_{xx}}{\partial x} + \frac{\partial \sigma_{xy}}{\partial y} + F_x &= 0 \\ \frac{\partial \sigma_{xy}}{\partial x} + \frac{\partial \sigma_{yy}}{\partial y} + F_y &= 0 \\ \frac{\partial \sigma_{xz}}{\partial x} + \frac{\partial \sigma_{yz}}{\partial y} + F_z &= 0 \end{aligned} \tag{1}$$

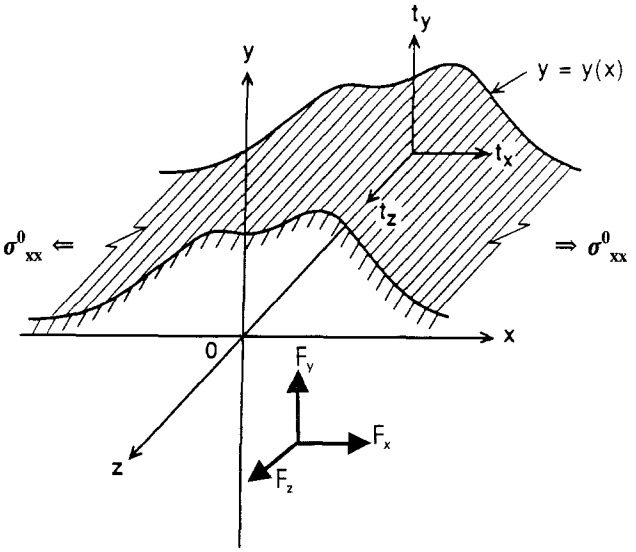

Fig. 1. Geometry of the problem. Half space limited by a boundary curve $y = y(x)$, and subject to body forces F_i $(i = x, y, z)$, surface tractions t_i $(i = x, y, z)$, and a uniform far-field stress field σ_{ij}^0 $(i, j = x, y, z)$. In this figure, only the component σ_{xx}^0 is shown for illustration

2.2 Constitutive relations

$$[e] = [a]\,[\sigma] \tag{2}$$

or

$$[\sigma] = [c]\,[e] \tag{3}$$

where

$$[e] = [\varepsilon_x, \varepsilon_y, \varepsilon_z, \gamma_{yz}, \gamma_{xz}, \gamma_{xy}]^T \tag{4}$$

are the strain components, and

$$[\sigma] = [\sigma_{xx}, \sigma_{yy}, \sigma_{zz}, \sigma_{yz}, \sigma_{xz}, \sigma_{xy}]^T \tag{5}$$

are the stress components, $[a]$ is a 6×6 symmetric compliance matrix with 21 independent components a_{ij} $(i, j = 1-6)$ and $[c]$ is the corresponding stiffness matrix with components c_{ij} $(i, j = 1-6)$ and is such that $[a] = [c]^{-1}$. In Eqs. (4) and (5), the superscript T indicates the transpose of the matrix.

2.3 Compatibility conditions

$$\begin{aligned} &\frac{\partial \gamma_{xz}}{\partial y} - \frac{\partial \gamma_{yz}}{\partial x} = 0 \\ &\frac{\partial^2 \varepsilon_x}{\partial y^2} + \frac{\partial^2 \varepsilon_y}{\partial x^2} = \frac{\partial^2 \gamma_{xy}}{\partial x\, \partial y} \end{aligned} \tag{6}$$

2.4 Boundary conditions on $y = y(x)$

$$\begin{aligned} &\sigma_{xx} \cos(n, x) + \sigma_{xy} \cos(n, y) = t_x \\ &\sigma_{xy} \cos(n, x) + \sigma_{yy} \cos(n, y) = t_y \\ &\sigma_{xz} \cos(n, x) + \sigma_{yz} \cos(n, y) = t_z \end{aligned} \tag{7}$$

where $\cos(n, x)$ and $\cos(n, y)$ are the direction cosines of the outward normal, $\boldsymbol{n}$, of the boundary curve $y = y(x)$.

3 Analytical method

Because the problem is linear, we can express the total stress field as the sum of the following three stress fields:

$$\sigma_{ij} = \sigma_{ij}^h + \sigma_{ij}^p + \sigma_{ij}^0. \tag{8}$$

In Eq. (8), σ_{ij}^0 is the given uniform stress field, and σ_{ij}^p is the particular solution of the stress field corresponding to the body force F_i in Eq. (1). This particular solution is required to satisfy the compatibility condition (6). One such particular solution is that corresponding to gravity which has been studied exclusively elsewhere [7], [8]. Finally, σ_{ij}^h is the homogeneous solution of Eq. (1)

which can be expressed in terms of three analytical functions as follows [7], [9]:

$$\begin{aligned}
\sigma_{xx}^h &= 2\,\mathrm{Re}\,[\mu_1^2\Phi_1'(z_1) + \mu_2^2\Phi_2'(z_2) + \mu_3^2\lambda_3\Phi_3'(z_3)]\\
\sigma_{yy}^h &= 2\,\mathrm{Re}\,[\Phi_1'(z_1) + \Phi_2'(z_2) + \lambda_3\Phi_3'(z_3)]\\
\sigma_{xy}^h &= -2\,\mathrm{Re}\,[\mu_1\Phi_1'(z_1) + \mu_2\Phi_2'(z_2) + \mu_3\lambda_3\Phi_3'(z_3)]\\
\sigma_{xz}^h &= 2\,\mathrm{Re}\,[\mu_1\lambda_1\Phi_1'(z_1) + \mu_2\lambda_2\Phi_2'(z_2) + \mu_3\Phi_3'(z_3)]\\
\sigma_{yz}^h &= -2\,\mathrm{Re}\,[\lambda_1\Phi_1'(z_1) + \lambda_2\Phi_2'(z_2) + \Phi_3'(z_3)]\\
\sigma_{zz}^h &= -\frac{2}{a_{33}}\,\mathrm{Re}\,\{[a_{13}\mu_1^2 + a_{23} - a_{34}\lambda_1 + a_{35}\mu_1\lambda_1 - a_{36}\mu_1]\,\Phi_1'(z_1)\\
&\quad + [a_{13}\mu_2^2 + a_{23} - a_{34}\lambda_2 + a_{35}\mu_2\lambda_2 - a_{36}\mu_2]\,\Phi_2'(z_2)\\
&\quad + [a_{13}\lambda_3\mu_3^2 + a_{23}\lambda_3 - a_{34} + a_{35}\mu_3 - a_{36}\mu_3\lambda_3]\,\Phi_3'(z_3)\}.
\end{aligned} \tag{9}$$

In Eq. (9): (i) μ_1, μ_2 and μ_3 are complex numbers with positive imaginary parts. These numbers and their respective conjugates are the roots of the following equation:

$$l_4(\mu)\,l_2(\mu) - l_3^2(\mu) = 0 \tag{10}$$

with

$$\begin{aligned}
l_2(\mu) &= \beta_{55}\mu^2 - 2\beta_{45}\mu + \beta_{44}\\
l_3(\mu) &= \beta_{15}\mu^3 - (\beta_{14} + \beta_{56})\,\mu^2 + (\beta_{25} + \beta_{46})\,\mu - \beta_{24}\\
l_4(\mu) &= \beta_{11}\mu^4 - 2\beta_{16}\mu^3 + (2\beta_{12} + \beta_{66})\,\mu^2 - 2\beta_{26}\mu + \beta_{22}.
\end{aligned} \tag{11}$$

β_{ij} $(i, j = 1-6)$ are related to the elements a_{ij} of matrix $[\boldsymbol{a}]$ in Eq. (2) as follows:

$$\beta_{ij} = a_{ij} - a_{i3}a_{j3}/a_{33} \qquad (i, j = 1, 2, 4, 5, 6). \tag{12}$$

(ii) λ_1, λ_2 and λ_3 are such that

$$\lambda_1 = -\frac{l_3(\mu_1)}{l_2(\mu_1)}; \qquad \lambda_2 = -\frac{l_3(\mu_2)}{l_2(\mu_2)}; \qquad \lambda_3 = -\frac{l_3(\mu_3)}{l_4(\mu_3)}. \tag{13}$$

(iii) $\Phi_k'(z_k)$ $(k = 1, 2, 3)$ denote the derivatives of three analytical functions $\Phi_k(z_k)$ with respect to the variable $z_k = x + \mu_k y$ where x and y are the coordinates of the point in the anisotropic medium at which the stresses are calculated. The three functions $\Phi_k(z_k)$ must satisfy the traction conditions along the boundary curve $y = y(x)$. Following a procedure similar to that used by Pan and Amadei [7], these traction conditions can be expressed as follows:

$$2\,\mathrm{Re}\,[\Phi_1(z_1) + \Phi_2(z_2) + \lambda_3\Phi_3(z_3)] = \int_0^s [t_y - (\sigma_{yy}^p + \sigma_{yy}^0)\,x'(s) + (\sigma_{xy}^p + \sigma_{xy}^0)\,y'(s)]\,ds \tag{14}$$

$$2\,\mathrm{Re}\,[\mu_1\Phi_1(z_1) + \mu_2\Phi_2(z_2) + \mu_3\lambda_3\Phi_3(z_3)] = \int_0^s [-t_x + (\sigma_{xy}^p + \sigma_{xy}^0)\,x'(s) - (\sigma_{xx}^p + \sigma_{xx}^0)\,y'(s)]\,ds \tag{15}$$

$$2\,\mathrm{Re}\,[\lambda_1\Phi_1(z_1) + \lambda_2\Phi_2(z_2) + \Phi_3(z_3)] = \int_0^s [-t_z + (\sigma_{yz}^p + \sigma_{yz}^0)\,x'(s) - (\sigma_{xz}^p + \sigma_{xz}^0)\,y'(s)]\,ds \tag{16}$$

where s is the arc-length along the curve $y = y(x)$. $x'(s)$ and $y'(s)$ are the total derivatives of x and y with respect to s, respectively.

The determination of the three functions $\Phi_k(z_k)$ and their derivatives depends mainly upon the geometry of the boundary curve $y = y(x)$. As shown by Pan and Amadei [7], these functions can be determined using a numerical conformal mapping method [10] and an integral equation method [11]. Three new analytical functions Ψ_k $(k = 1, 2, 3)$ are introduced such that

$$\Psi_k'(\zeta_k) = \Phi_k'(z_k)\, Z_k'(\zeta_k) \quad (k = 1, 2, 3) \tag{17}$$

where $z_k = Z_k(\zeta_k)$ $(k = 1, 2, 3)$ are three conformal mapping functions that map the lower half planes bounded by $z_k = x(t) + \mu_k y(t)$ onto the lower flat half planes $\operatorname{Im} \zeta_k \leqq 0$ $(k = 1, 2, 3)$ [7]. In Eq. (17), $\Psi_k'(\zeta_k)$ and $Z_k'(\zeta_k)$ are the derivatives of Ψ_k and Z_k with respect to ζ_k. Let t_k be the boundary value of ζ_k, and following a procedure similar to that used by Pan and Amadei [7], it can be shown that the boundary conditions (14)–(16) lead to the following system of three singular integral equations that can be solved for the three functions $\Psi_k'(t_k)$:

$$b_{11}\Psi_1'(\tau_1) + \frac{b_{12}}{2}\Psi_2'(\tau_2)\, t_2'(\tau_1) + \frac{b_{13}}{2}\Psi_3'(\tau_3)\, t_3'(\tau_1)$$

$$+ \frac{b_{12}}{2\pi i}\int_{+\infty}^{-\infty} \frac{\Psi_2'(t_2)\, t_2'(t_1)\, dt_1}{t_1 - \tau_1} + \frac{b_{13}}{2\pi i}\int_{+\infty}^{-\infty} \frac{\Psi_3'(t_3)\, t_3'(t_1)\, dt_1}{t_1 - \tau_1}$$

$$= \frac{f_1(\tau)\, t'(\tau_1)}{2} + \frac{1}{2\pi i}\int_{+\infty}^{-\infty} \frac{f_1(t)\, t'(t_1)\, dt_1}{t_1 - \tau_1} \tag{18}$$

$$b_{21}\Psi_2'(\tau_2) + \frac{b_{22}}{2}\Psi_1'(\tau_1)\, t_1'(\tau_2) + \frac{b_{23}}{2}\Psi_3'(\tau_3)\, t_3'(\tau_2)$$

$$+ \frac{b_{22}}{2\pi i}\int_{+\infty}^{-\infty} \frac{\Psi_1'(t_1)\, t_1'(t_2)\, dt_2}{t_2 - \tau_2} + \frac{b_{23}}{2\pi i}\int_{+\infty}^{-\infty} \frac{\Psi_3'(t_3)\, t_3'(t_2)\, dt_2}{t_2 - \tau_2}$$

$$= \frac{f_2(\tau)\, t'(\tau_2)}{2} + \frac{1}{2\pi i}\int_{+\infty}^{-\infty} \frac{f_2(t)\, t'(t_2)\, dt_2}{t_2 - \tau_2} \tag{19}$$

$$b_{31}\Psi_3'(\tau_3) + \frac{b_{32}}{2}\Psi_1'(\tau_1)\, t_1'(\tau_3) + \frac{b_{33}}{2}\Psi_2'(\tau_2)\, t_2'(\tau_3)$$

$$+ \frac{b_{32}}{2\pi i}\int_{+\infty}^{-\infty} \frac{\Psi_1'(t_1)\, t_1'(t_3)\, dt_3}{t_3 - \tau_3} + \frac{b_{33}}{2\pi i}\int_{+\infty}^{-\infty} \frac{\Psi_2'(t_2)\, t_2'(t_3)\, dt_3}{t_3 - \tau_3}$$

$$= \frac{f_3(\tau)\, t'(\tau_3)}{2} + \frac{1}{2\pi i}\int_{+\infty}^{-\infty} \frac{f_3(t)\, t'(t_3)\, dt_3}{t_3 - \tau_3} \tag{20}$$

where the coefficients b_{ij} $(i, j = 1, 2, 3)$ and the functions $f_i(t)$ $(i = 1, 2, 3)$ are given by Eqs. (A.1) and (A.2) in Appendix A. In Eqs. (18)–(20), τ is a fixed point on the t $[-\infty, +\infty]$ axis and τ_k $(k = 1, 2, 3)$ are fixed points on the t_k $(\operatorname{Im} \zeta_k = 0)$ axes. $t'(t_j)$ and $t_k'(t_j)$ $(k, j = 1, 2, 3)$ are respectively the total derivatives of t and t_k with respect to the variable t_j $[-\infty, +\infty]$ and are

equal to

$$t'(t_j) = \frac{Z_j'(t_j)}{x'(t) + \mu_j y'(t)}; \quad t_k'(t_j) = \frac{Z_j'(t_j)}{Z_k'(t_k)} \cdot \frac{x'(t) + \mu_k y'(t)}{x'(t) + \mu_j y'(t)} \tag{21}$$

where $x'(t)$ and $y'(t)$ are the derivatives of x and y with respect to t, respectively.

The three integral equations (18)–(20) can be discretized and solved for the boundary values of the three analytical functions $\Psi_k'(t_k)$ by the method proposed by Sarkar et al. [13]. Then, the interior values of these analytical functions are calculated using the Cauchy integral theorem [11]. Finally, the stress functions $\Phi_k'(z_k)$ are obtained using Eq. (17) and the six stress components are determined using Eqs. (8) and (9). The infinite integrals appearing in Eqs. (19)–(21) are determined using an inverse mapping from the boundary of the ζ_k planes to the circumference of unit discs [7]. It is also noted that for these integrals to converge, the boundary curve $(x(t), y(t))$, the surface tractions and the body forces must be such that the following limits exist:

$$\begin{gathered}
\lim_{t \to \pm\infty} |t_i s'(t)| < \infty \\
\lim_{t \to \pm\infty} |x'(t)| < \infty; \quad \lim_{t \to \pm\infty} |y'(t)| < \infty \\
\lim_{t \to \pm\infty} |\sigma_{ij}^p x'(t)| < \infty; \quad \lim_{t \to \pm\infty} |\sigma_{ij}^p y'(t)| < \infty.
\end{gathered} \tag{22}$$

4 Generalized plane strain, plane and antiplane problems

The half space with the geometry of Fig. 1 is assumed to be *orthotropic* in an n, s, t Cartesian coordinate system attached to planes of anisotropy in the medium. The orientation of that local coordinate system with respect to the global x, y, z coordinate system is defined by a dip azimuth β and a dip angle ψ as shown in Fig. 2. The t-axis is located in the xz plane. The constitutive equation in the n, s, t coordinate system is given by the following equation [9]:

$$\begin{bmatrix} \varepsilon_n \\ \varepsilon_s \\ \varepsilon_t \\ \gamma_{st} \\ \gamma_{nt} \\ \gamma_{ns} \end{bmatrix} = \begin{bmatrix} \frac{1}{E_n} & -\frac{\nu_{sn}}{E_s} & -\frac{\nu_{tn}}{E_t} & 0 & 0 & 0 \\ -\frac{\nu_{ns}}{E_n} & \frac{1}{E_s} & -\frac{\nu_{ts}}{E_t} & 0 & 0 & 0 \\ -\frac{\nu_{nt}}{E_n} & -\frac{\nu_{st}}{E_s} & \frac{1}{E_t} & 0 & 0 & 0 \\ 0 & 0 & 0 & \frac{1}{G_{st}} & 0 & 0 \\ 0 & 0 & 0 & 0 & \frac{1}{G_{nt}} & 0 \\ 0 & 0 & 0 & 0 & 0 & \frac{1}{G_{ns}} \end{bmatrix} \begin{bmatrix} \sigma_{nn} \\ \sigma_{ss} \\ \sigma_{tt} \\ \sigma_{st} \\ \sigma_{nt} \\ \sigma_{ns} \end{bmatrix} \tag{23}$$

or in a more compact matrix form as

$$[e]_{nst} = [h]\,[\sigma]_{nst}. \tag{24}$$

In Eq. (23), E_n, E_s and E_t are, respectively, Young's moduli in the n, s and t directions, respectively. G_{ns}, G_{nt} and G_{st} are, respectively, the shear moduli in planes parallel to the ns, nt and st

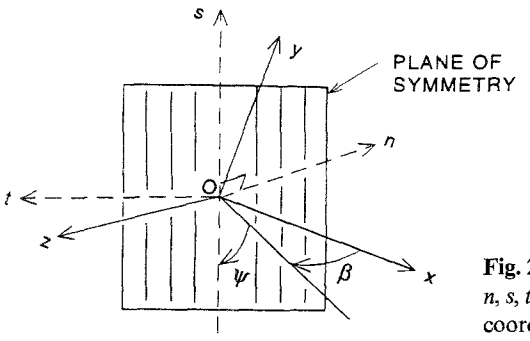

Fig. 2. Orientation of planes of symmetry (i.e. the local n, s, t coordinate system) with respect to the global x, y, z coordinate system

planes, respectively. Finally, v_{ij} $(i, j = n, s, t)$ are Poisson's ratios that characterize the normal strains in the symmetry directions j when a stress is applied in the symmetry directions i. Because of symmetry of the compliance matrix $[\boldsymbol{h}]$, Poisson's ratios v_{ij} and v_{ji} are such that $v_{ij}/E_i = v_{ji}/E_j$. Therefore, nine independent elastic constants are needed to describe the deformability of the material in the local n, s, t coordinate system.

For known orientations of the planes of anisotropy with respect to the x, y, and z axes, the compliance matrix $[\boldsymbol{a}]$ of Eq. (2) in the global (x, y, z) coordinate system can be obtained by using second order tensor coordinate transformation rules [9], [14]. Actually, a linear relationship exists between the elements of matrix $[\boldsymbol{a}]$ in Eq. (2) and the elements of matrix $[\boldsymbol{h}]$ in Eq. (24), which can be expressed as

$$[\boldsymbol{a}] = [\boldsymbol{Q}]^T [\boldsymbol{h}] [\boldsymbol{Q}] \tag{25}$$

where $[\boldsymbol{Q}]$ is a 6×6 matrix given in Appendix B.

Because of this linear relationship, one can show that the total stresses in their dimensionless form depend on the following eight dimensionless quantities:

$$\frac{E_s}{E_n};\quad \frac{E_s}{E_t};\quad v_{sn};\quad v_{tn};\quad v_{ts};\quad \frac{E_s}{G_{st}};\quad \frac{E_s}{G_{nt}};\quad \frac{E_s}{G_{ns}}. \tag{26}$$

If the medium in the local (n, s, t) coordinate system is *transversely isotropic* in one of the three ns, nt or st planes, only five independent elastic constants E, E', v, v' and G' are needed to describe the deformability of the medium in the n, s, t coordinate system where: (i) E and E' are Young's moduli in the plane of transverse isotropy and in the direction normal to it, respectively, (ii) v and v' are Poisson's ratios characterizing the lateral strain response in the plane of transverse isotropy to a stress acting parallel and normal to it, respectively, and, (iii) G' is the shear modulus in planes normal to the plane of transverse isotropy. Again, for this case, the total stresses in their dimensionless forms are found to depend on the following four dimensionless terms:

$$\frac{E}{E'};\quad v;\quad v';\quad \frac{G}{G'}. \tag{27}$$

It is obvious that the total stresses in their dimensionless form also depend on (i) the orientation angles β and ψ of the planes of anisotropy with respect to the x-, y- and z-axes of Fig. 1, (ii) the coordinates of the points at which the stresses are calculated, (iii) the geometry of the surface morphology, and (iv) the relative magnitudes of the surface tractions, body forces, and the uniform far-field stresses. Equations (8) and (9) show that, in general, at each point in the half space, the stress field is three dimensional and the principal stress components are inclined with respect to the x, y and z axes.

The generalized plane strain solution presented above takes a simpler form for orthotropic and transversely isotropic materials with planes of elastic symmetry normal to the z axis of Fig. 1. This takes place (i) when the dip azimuth β in Fig. 2 is zero and the dip angle ψ varies between 0 and 90 degrees or (ii) when β and ψ are equal to 90 degrees. For those cases the generalized plane strain solution reduces to a plane strain solution with

$$\begin{aligned} &c_{46} = c_{56} = c_{4i} = c_{5i} = 0 \quad \text{for } i = 1, 2, 3 \\ &\beta_{46} = \beta_{56} = \beta_{4i} = \beta_{5i} = 0 \quad \text{for } i = 1, 2, 3 \\ &l_3(\mu) = \lambda_1 = \lambda_2 = \lambda_3 = 0 \end{aligned} \tag{28}$$

and the problem of finding the total stresses can be decomposed as the sum of two uncoupled problems:

(i) *a plane problem* for which the stress components are equal to

$$\begin{aligned} \sigma_{xx} &= 2\,\mathrm{Re}\,[\mu_1^2\Phi_1'(z_1) + \mu_2^2\Phi_2'(z_2)] + \sigma_{xx}^p + \sigma_{xx}^0 \\ \sigma_{yy} &= 2\,\mathrm{Re}\,[\Phi_1'(z_1) + \Phi_2'(z_2)] + \sigma_{yy}^p + \sigma_{yy}^0 \\ \sigma_{xy} &= -2\,\mathrm{Re}\,[\mu_1\Phi_1'(z_1) + \mu_2\Phi_2'(z_2)] + \sigma_{xy}^p + \sigma_{xy}^0 \\ \sigma_{zz} &= -\frac{2}{a_{33}}\,\mathrm{Re}\,\{[a_{13}\mu_1^2 + a_{23} - a_{36}\mu_1]\,\Phi_1'(z_1) + [a_{13}\mu_2^2 + a_{23} - a_{36}\mu_2]\,\Phi_2'(z_2)\} + \sigma_{zz}^p + \sigma_{zz}^0 \end{aligned} \tag{29}$$

where μ_1 and μ_2 are the roots of $l_4(\mu) = 0$ in Eq. (11), and $\Phi_k'(z_k)$ are related to $\Psi_k'(\zeta_k)$ $(k = 1, 2)$ through Eq. (17). The boundary values of the latter functions $\Psi_1'(t_1)$ and $\Psi_2'(t_2)$ are obtained by solving the two integral equations (18) and (19) with b_{ij} and $f_i(t)$ defined in Eqs. (A.4) and (A.5) in Appendix A.

(ii) *An antiplane problem* for which the total stress components are equal to

$$\begin{aligned} \sigma_{xz} &= 2\,\mathrm{Re}\,[\mu_3\Phi_3'(z_3)] + \sigma_{xz}^p + \sigma_{xz}^0 \\ \sigma_{yz} &= -2\,\mathrm{Re}\,[\Phi_3'(z_3)] + \sigma_{yz}^p + \sigma_{yz}^0. \end{aligned} \tag{30}$$

Similarly, μ_3 is the root of $l_2(\mu) = 0$ in Eq. (11), and $\Phi_3'(z_3)$ is related to $\Psi_3'(\zeta_3)$ through Eq. (17). The boundary values of the latter function $\Psi_3'(t_3)$ are obtained from the integral equation (20).

5 Surface morphologies

The half-space's surface morphology is assumed to be smooth and to be expressed in parametric form as follows:

$$\begin{aligned} &x(t) = t \quad (-\infty < t < +\infty) \\ &y(t) = \sum_{i=1}^{N} y_i(t) \end{aligned} \tag{31}$$

with

$$y_i(t) = \frac{a_i^2 b_i}{(t - x_i)^2 + a_i^2}. \tag{32}$$

Equations (31) and (32) correspond to the geometric superposition of $i = 1, N$ symmetric ridges or valleys $x(t)$, $y_i(t)$ centered at $x = x_i$. If b_i is positive, Eq. (32) corresponds to a ridge with height b_i (see Fig. 3a for $a_i/b_i = 1$). If b_i is negative, Eq. (32) corresponds to a valley with depth $|b_i|$ (see Fig. 3b for $a_i/b_i = -1$). The parameter a_i controls the lateral extent of each ridge or valley with inflection points located at $x = x_i \pm a_i/\sqrt{3}$, $y = 0.75b_i$ at which the slopes are equal to $\pm 3b_i\sqrt{3}/(8a_i)$ [7]. Thus, any given smooth morphologies can be expressed by choosing different positive or negative values of a_i, b_i and x_i for $i = 1, N$. As an example, Fig. 4 shows the geometry (in dimensionless form) of three symmetric valleys with $N = 1, x_1 = 0$, and $a_1/b_1 = -2, -1$, and -0.5. The respective slopes at the inflection points of the valleys are equal to ± 0.32 (18.0°), ± 0.65 (33.0°), and ± 1.30 (52.4°).

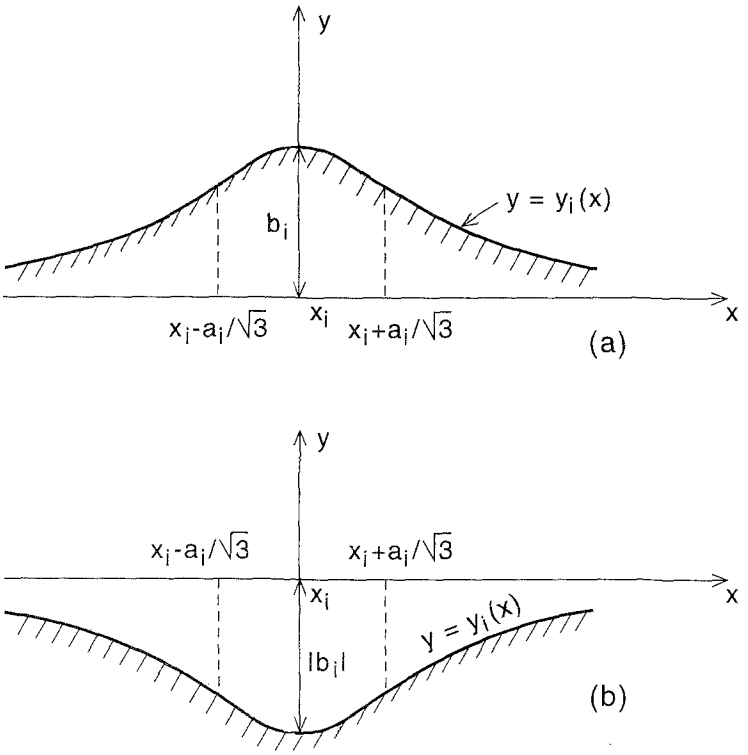

Fig. 3. Symmetric surface morphologies centered at $x = x_i$. **a** A symmetric ridge of height b_i with $a_i/b_i = 1$, **b** a symmetric valley of depth $|b_i|$ with $a_i/b_i = -1$

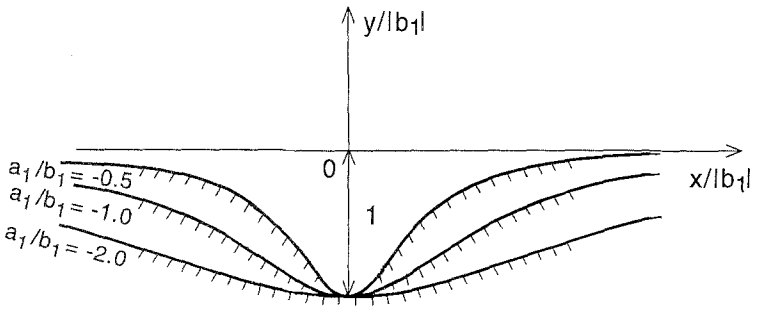

Fig. 4. Symmetric valleys with $x_1 = 0$, and $a_1/b_1 = -2, -1$ and -0.5

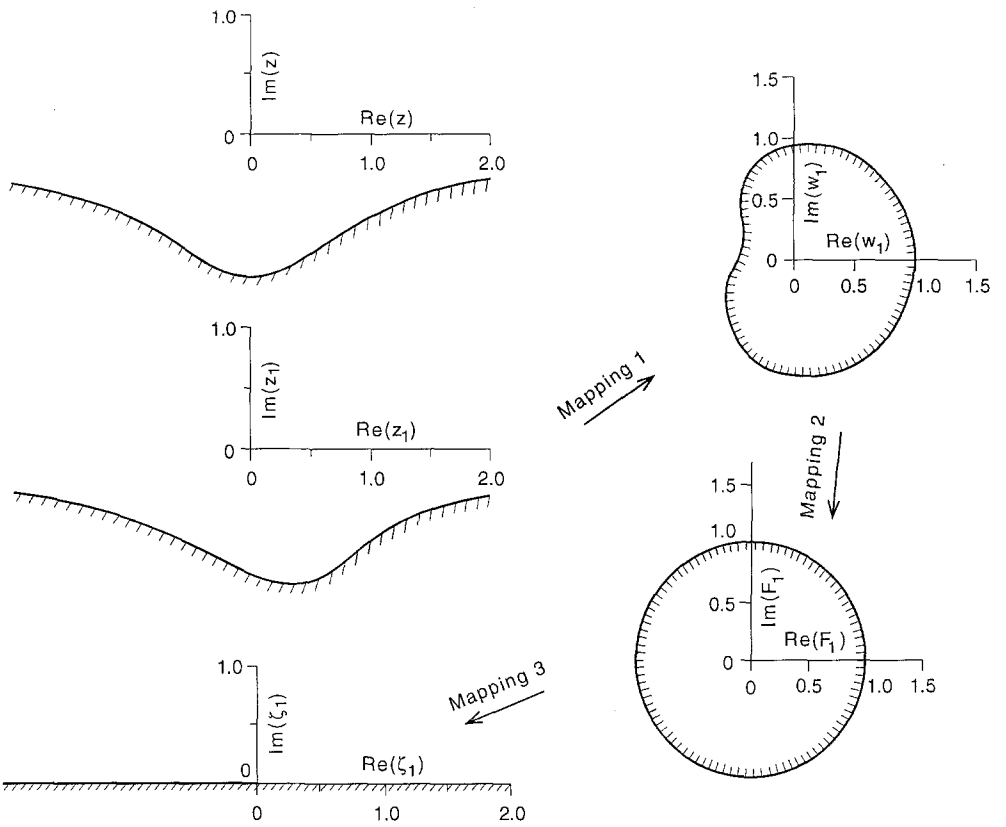

Fig. 5. Example of mappings 1, 2, and 3 for $k = 1$ and for the symmetric valley of Fig. 3 b. Other parameters are: dip azimuth $\beta = 0°$, dip angle $\psi = 45°$, and $E/E' = G/G' = 3$, $\nu = 0.25$, $\nu' = 0.15$

For the surface morphology defined in Eqs. (31) and (32), the mappings $z_k = Z_k(\zeta_k)$ $(k = 1, 2, 3)$ which map the lower half planes bounded by $z_k = x(t) + \mu_k y(t)$ onto the flat lower half planes $\text{Im}\,\zeta_k \leqq 0$ $(k = 1, 2, 3)$ consist of three successive conformal mappings (Fig. 5):

Mapping 1:

$$z_k \Rightarrow w_k \qquad k = 1, 2, 3$$

$$w_k(t) = \frac{z_k(t) + iA_k}{z_k(t) - iA_k} \qquad -\infty < t < \infty \tag{33}$$

with

$$z_k(t) = t + \mu_k \sum_{i=1}^{N} a_i^2 b_i / ((t - x_i)^2 + a_i^2) \tag{34}$$

maps the lower half planes bounded by $z_k = x(t) + \mu_k y(t)$ onto irregular bounded domains w_k. In Eq. (33), A_k $(k = 1, 2, 3)$ are complex constants chosen such that the mapping is conformal. The variable t in Eq. (33) can be replaced by a new parameter θ that varies over a finite interval $[-\pi/2, \pi/2]$ such that $t = \tan\theta$. Then Eq. (33) takes the following form:

$$w_k(\theta) = \frac{p(\theta) + iA_k \cos\theta}{p(\theta) - iA_k \cos\theta} \qquad k = 1, 2, 3; \quad -\frac{\pi}{2} < \theta < \frac{\pi}{2} \tag{35}$$

with

$$p(\theta) = \sin\theta + \mu_k \sum_{i=1}^{N} \frac{a_i^2 b_i \cos^3\theta}{(\sin\theta - x_i \cos\theta)^2 + a_i^2 \cos^2\theta}. \tag{36}$$

Mapping 2:

$$\begin{aligned} &w_k \Rightarrow F_k \qquad k = 1, 2, 3 \\ &F_k = F_k(w_k) \end{aligned} \tag{37}$$

maps the irregular bounded domains w_k onto unit discs F_k. This is done using a numerical conformal mapping method as discussed in Trummer [10] and Pan and Amadei [7].

Mapping 3:

$$\begin{aligned} &F_k \Rightarrow \zeta_k \qquad k = 1, 2, 3 \\ &\zeta_k = i \frac{F_k(w_k) + 1}{F_k(w_k) - 1} \end{aligned} \tag{38}$$

maps the unit discs F_k onto the flat half-planes ζ_k.

For the morphology defined in Eqs. (31) and (32), $t'(t_j)$ and $t_k'(t_j)$ defined in Eq. (21) take the following forms:

$$\begin{aligned} t'(t_j) &= \frac{Z_j'(t_j)}{1 - 2\mu_j q(t)} \\ t_k'(t_j) &= \frac{Z_j'(t_j)}{Z_k'(t_k)} \cdot \frac{1 - 2\mu_k q(t)}{1 - 2\mu_j q(t)} \end{aligned} \tag{39}$$

with

$$q(t) = \sum_{i=1}^{N} \frac{a_i^2 b_i (t - x_i)}{[(t - x_i)^2 + a_i^2]^2}. \tag{40}$$

6 Numerical examples

In the following numerical examples, stress concentration at the irregular surface of a half-space is analyzed. The half-space consists of either an isotropic or a transversely isotropic medium, and is subjected to a far-field horizontal stress σ_{xx}^0. In the transversely isotropic case, the planes of transverse isotropy are assumed to be parallel to the z-axis of Fig. 1 ($\beta = 0°$), and the elastic constants of the medium are selected within the following restrictions [14], [15]:

$$\begin{aligned} &E, E', G, G' > 0 \\ &0 \leqq \nu < 1 \\ &1 - \nu - 2\nu'^2 \frac{E}{E'} > 0. \end{aligned} \tag{41}$$

Note that since the anisotropic solution presented in this paper cannot be reduced directly to the isotropic solution [7], a nearly isotropic material (NI) with $E/E' = G/G' = 1$, $\nu = 0.25$, $\nu' = 0.24$,

and $\psi = 0°$ is adopted. It is also noted that in Figs. 7, 9, and 10, only the right halves of the plots are presented because of symmetry.

Figures 6–9 show how the stress concentration (or normalized horizontal stress), $\sigma_{xx}/\sigma^0_{xx}$, varies with the normalized horizontal distance $x/|b_1|$ along the surface of a symmetric valley with the geometry of Fig. 3b.

Figure 6 shows the effect of the dip angle, ψ, of the planes of transverse isotropy on the stress concentration. The medium's elastic properties are such that $E/E' = G/G' = 3$, $\nu = 0.25$, $\nu' = 0.15$, and the dip angle $\psi = 0$, 45, or 90 degrees. The nearly isotropic case (NI) is also shown for comparison. It is clear from Fig. 6 that near the central region of the valley ($|x|/|b_1| \leqq 0.5$), the magnitude of the horizontal stress is usually higher than the magnitude of the far-field horizontal stress. The maximum value of $\sigma_{xx}/\sigma^0_{xx}$ along the surface of the valley, defined here as the stress concentration factor (SCF), is greater than 3 for the transversely isotropic and nearly isotropic cases. Actually, SCF = 5.4, 3.3, and 3.4, respectively, for $\psi = 0$, 45, and 90 degrees, compared to 3.7 for the nearly isotropic case. Notice that for $\psi = 45$ degrees, the SCF is reached not at the center, but on the left-hand side of the valley ($|x|/|b_1| = -0.08$). Figure 6 indicates that in order to reduce the SCF, horizontal planes of transverse isotropy should be avoided. Also for non-horizontal planes of transverse isotropy, the SCF can be smaller than its value for the isotropic case.

Figures 7–9 show the effect of the degree of anisotropy on the stress concentration. Again, the nearly isotropic case (NI) is included for comparison. In Fig. 7, the medium's elastic properties are such that $G/G' = 3$, $\nu = 0.25$, $\nu' = 0.15$, $\psi = 0°$, with E/E' equal to 1, 2 or 3. It can be seen from this figure that the three curves corresponding to $E/E' = 1, 2, 3$ nearly coincide with each other, which implies that the value of Young's modulus ratio does not have much influence on the stress concentration (for instance, SCF = 5.2, 5.3, and 5.4, for $E/E' = 1$, 2, and 3, respectively, a slight increase with increasing E/E'). However, these SCF values are significantly different from the value of 3.7 associated with the nearly isotropic case. In Fig. 8, the medium's elastic properties are such that $E/E' = 3$, $\nu = 0.25$, $\nu' = 0.15$, $\psi = 45°$, with G/G' equal to 1, 2 or 3.

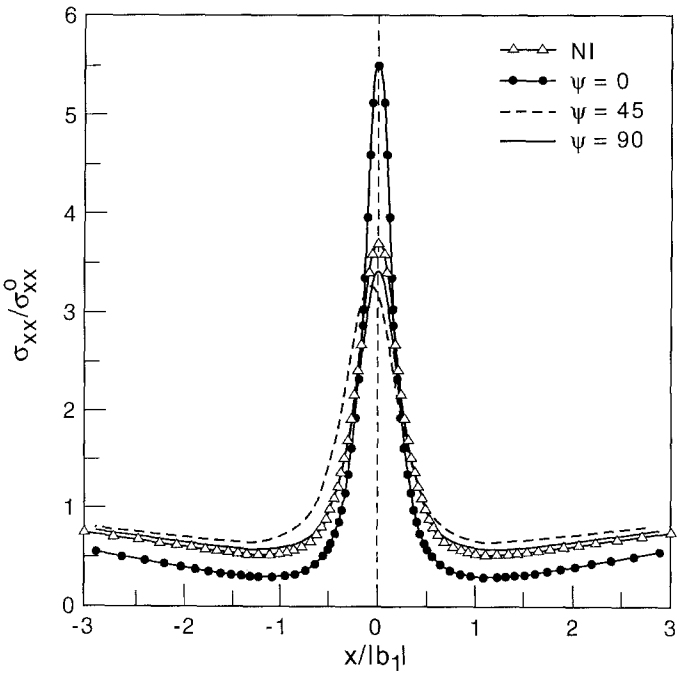

Fig. 6. Variation of the stress concentration $\sigma_{xx}/\sigma^0_{xx}$ along the surface of a symmetric valley with $x_1 = 0$ and $a_1/b_1 = -1$. The material properties are such that $E/E' = G/G' = 3$, $\nu = 0.25$, $\nu' = 0.15$. The dip angle of the planes of transverse isotropy $\psi = 0$, 45, or 90 degrees. The stress distribution for the nearly isotropic case (NI) is also shown for comparison

This figure shows that the value of the shear modulus ratio G/G' has a clear effect on the stress concentration. For example, the SCF decreases with increasing G/G' (SCF = 4.3, 3.7, and 3.3, for $G/G' = 1$, 2, and 3, respectively). It is also interesting to note that the SCF for the transversely isotropic case can be larger than, equal to, or smaller than the SCF for the nearly isotropic case. In Fig. 9, the medium's elastic properties are such that $E/E' = G/G' = 3$, $\nu = 0.25$, $\psi = 90°$, and

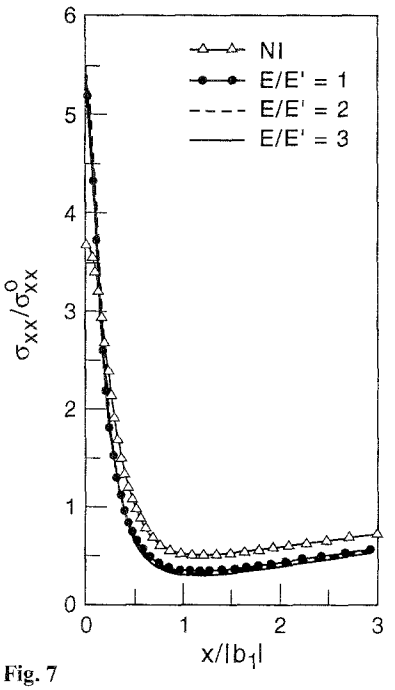

Fig. 7

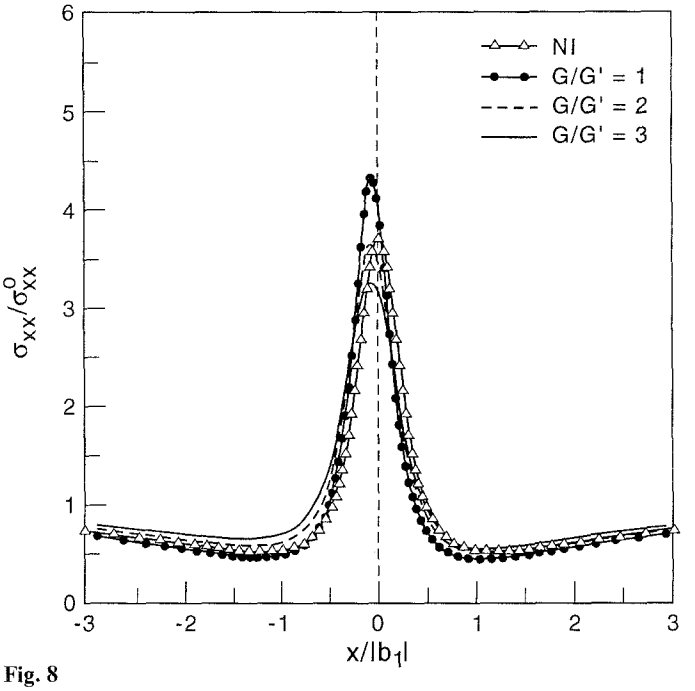

Fig. 8

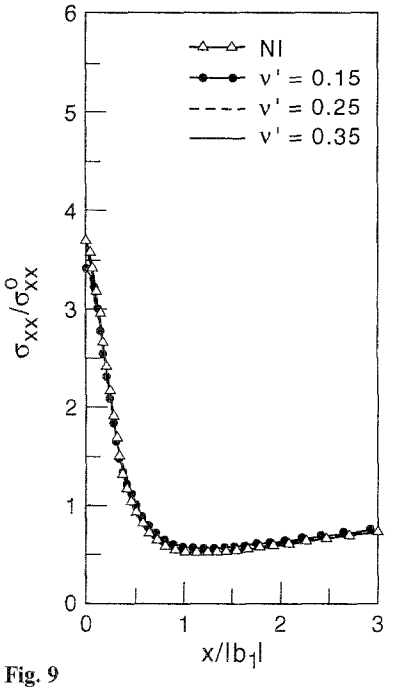

Fig. 9

Figs. 7–9. Variation of the stress concentration $\sigma_{xx}/\sigma^0_{xx}$ along the surface of a symmetric valley with $x_1 = 0$ and $a_1/b_1 = -1$. The transversely isotropic properties are such that $G/G' = 3$, $\nu = 0.25$, $\nu' = 0.15$, $\psi = 0$ degrees, and $E/E' = 1$, 2, and 3 **(Fig. 7)**, $E/E' = 3$, $\nu = 0.25$, $\nu' = 0.15$, $\psi = 45$ degrees, and $G/G' = 1$, 2, and 3 **(Fig. 8)**, and $E/E' = G/G' = 3$, $\nu = 0.25$, $\psi = 90$ degrees, and $\nu' = 0.15$, 0.25, and 0.35 **(Fig. 9)**. The stress distributions for the nearly isotropic case (NI) are also shown for comparison

$v' = 0.15$, 0.25 or 0.35. This figure shows that Poisson's ratio v' has little effect on the stress concentration. The SCF increases slightly with Poisson's ratio v' (SCF = 3.4, 3.5, and 3.6, for $v' = 0.15$, 0.25, and 0.35, respectively), and is slightly less than the value of 3.7 associated with the nearly isotropic case.

Figure 10 shows the effect of different surface profiles on the stress concentration. The medium's elastic properties are such that $E/E' = G/G' = 3$, $v = 0.25$, $v' = 0.15$, and $\psi = 90°$. The surface morphologies correspond to the three symmetric valleys shown in Fig. 4 with $a_1/b_1 = -2$, -1, and -0.5. Figure 10 clearly indicates that the geometry of the surface profiles has a great effect on the stress concentration, and that the SCF increases significantly with increasing a_1/b_1, corresponding to steeper valleys. For instance, for $a_1/b_1 = -2$, -1, and -0.5, SCF = 2, 3, and 6, respectively.

Finally, Fig. 11 shows the variation of the stress concentration $\sigma_{xx}/\sigma^0_{xx}$ along a complex surface. The half-space's morphology is obtained by superposition of $N = 4$ ridges and valleys of Eqs. (31) and (32). The parameters are $a_i/y(0) = 1$ for $i = 1-4$, $b_1/y(0) = 0.8983$, $b_2/y(0) = 1.2657$, $b_3/y(0) = -2.1186$, $b_4/y(0) = 1.3438$, $x_1/y(0) = 0$, $x_2/y(0) = 1.35$, $x_3/y(0) = 1.6$, and $x_4/y(0) = 2.1$. Here, $y(0)$ is the characteristic height of the surface morphology at $x = 0$. The

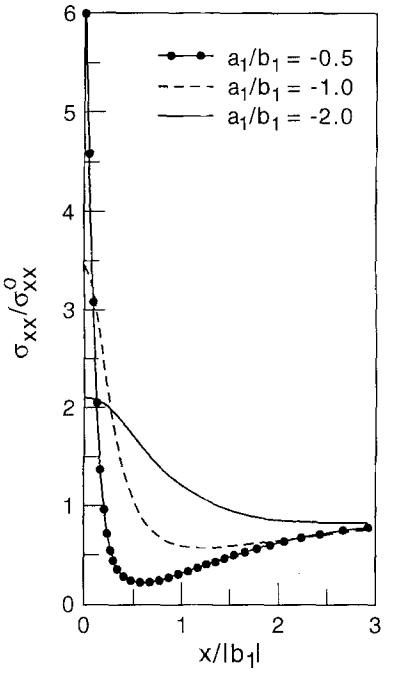

Fig. 10. Variation of the stress concentration $\sigma_{xx}/\sigma^0_{xx}$ along the surface of the symmetric valleys of Fig. 4 with $x_1 = 0$ and $a_1/b_1 = -2$, -1, -0.5. The transversely isotropic properties are such that $E/E' = G/G' = 3$, $v = 0.25$, $v' = 0.15$, and $\psi = 90$ degrees

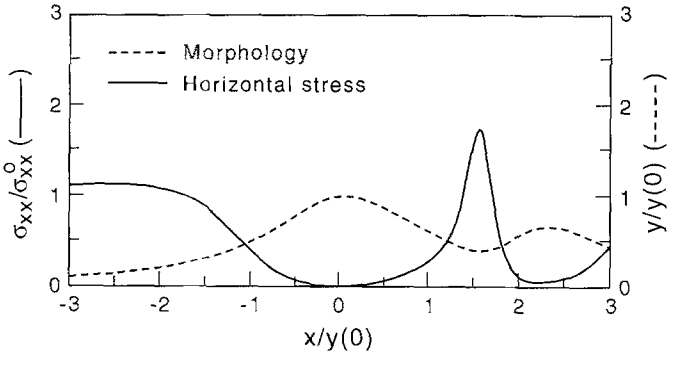

Fig. 11. Variation of the stress concentration $\sigma_{xx}/\sigma^0_{xx}$ (solid line) along the surface (dash line) of a half-space with complex morphology obtained by superposition of $N = 4$ ridges and valleys. The transversely isotropic properties are such that $E/E' = 2$, $G/G' = 1$, $v = v' = 0.25$, and the dip angle $\psi = 30$ degrees

medium's elastic properties are such that $E/E' = 2$, $G/G' = 1$, $\nu = \nu' = 0.25$, and the dip angle $\psi = 30$ degrees. Figure 11 shows clearly that the variation of the stress concentration along the surface is opposite to the geometry of the surface morphology, that is, local depressions (mounds) correspond to higher (lower) stress concentrations. For example, at $x/y(0) = 1.55$ (depression), the stress concentration is 1.72, while at $x/y(0) = 0$ (mound), the stress concentration is 0.

7 Conclusions

In this paper, an analytical method is presented to derive the stresses in an anisotropic half-space with a smooth and irregular surface consisting of the superposition of multiple long and symmetric ridges and valleys. The method overcomes the small amplitude morphology limitation associated with the perturbation method, and the isotropic and simple surface profile limitations related to the exact conformal mapping methods. The anisotropic half-space can be subjected to the combined effect of body forces, surface tractions, and uniform far-field stresses, which is an extension of the authors' previous results to the general case of body forces and far-field stresses. It is found that, in general, the stress field in the anisotropic half-space is three-dimensional (i.e. generalized plane strain) with the principal stresses being inclined with respect to the ridge or valley axis. However, for materials with higher degrees of elastic symmetry, the generalized plane strain solution can be decoupled into plane and antiplane problems.

As illustrative examples, the present solution was applied to find the stress concentration at irregular surfaces induced by a uniform far-field horizontal stress in transversely isotropic and isotropic media. It is found that while the half-space surface geometry and the orientation of the planes of material anisotropy can have a large effect on the stress concentration, the degree of material anisotropy has a lesser influence. For almost all the cases corresponding to symmetric valleys, the stress concentration factors are greater than 3, and can be as high as 5 or 6 if the far-field stress is parallel to the planes of transverse isotropy or if the surface morphology becomes steeper. For complex surface morphologies, the variation of the stress concentration along the surface is usually opposite to the geometry of the corresponding surface morphology, that is, local depressions (mounds) usually correspond to higher (lower) stress concentrations.

Appendix A

Coefficients b_{ij} and functions $f_i(t)$ in Eqs. (18)–(20):

$$
\begin{aligned}
b_{11} &= (\overline{\mu_2} - \mu_1)(\overline{\lambda_2\lambda_3} - 1) - (\overline{\mu_2 - \mu_3})\,\overline{\lambda_3}(\overline{\lambda_2} - \lambda_1)\\
b_{12} &= (\overline{\mu_2} - \mu_2)(\overline{\lambda_2\lambda_3} - 1) - (\overline{\mu_2 - \mu_3})\,\overline{\lambda_3}(\overline{\lambda_2} - \lambda_2)\\
b_{13} &= (\overline{\mu_2} - \mu_3)\,\lambda_3(\overline{\lambda_2\lambda_3} - 1) - (\overline{\mu_2 - \mu_3})\,\overline{\lambda_3}(\overline{\lambda_2}\lambda_3 - 1)\\
b_{21} &= (\overline{\lambda_1\lambda_3} - 1)(\overline{\mu_1} - \mu_2) - (\overline{\lambda_1} - \lambda_2)\,\overline{\lambda_3}(\overline{\mu_1 - \mu_3})\\
b_{22} &= (\overline{\lambda_1\lambda_3} - 1)(\overline{\mu_1} - \mu_1) - (\overline{\lambda_1} - \lambda_1)\,\overline{\lambda_3}(\overline{\mu_1 - \mu_3})\\
b_{23} &= (\overline{\lambda_1\lambda_3} - 1)\,\lambda_3(\overline{\mu_1} - \mu_3) - (\overline{\lambda_1}\lambda_3 - 1)\,\overline{\lambda_3}(\overline{\mu_1 - \mu_3})\\
b_{31} &= (\overline{\lambda_1 - \lambda_2})\,\lambda_3(\overline{\mu_1} - \mu_3) - (\overline{\lambda_1}\lambda_3 - 1)(\overline{\mu_1 - \mu_2})\\
b_{32} &= (\overline{\lambda_1 - \lambda_2})(\overline{\mu_1} - \mu_1) - (\overline{\lambda_1} - \lambda_1)(\overline{\mu_1 - \mu_2})\\
b_{33} &= (\overline{\lambda_1 - \lambda_2})(\overline{\mu_1} - \mu_2) - (\overline{\lambda_1} - \lambda_2)(\overline{\mu_1 - \mu_2})
\end{aligned}
\qquad \text{(A.1)}
$$

$$
\begin{aligned}
f_1(t) &= [\overline{\mu_2}(\overline{\lambda_2\lambda_3} - 1) - (\overline{\mu_2 - \mu_3})\,\overline{\lambda_2\lambda_3}]\,u(t) + (\overline{\lambda_2\lambda_3} - 1)\,v(t) - (\overline{\mu_2 - \mu_3})\,\overline{\lambda_3}w(t)\\
f_2(t) &= [\overline{\mu_1}(\overline{\lambda_1\lambda_3} - 1) - (\overline{\mu_1 - \mu_3})\,\overline{\lambda_1\lambda_3}]\,u(t) + (\overline{\lambda_1\lambda_3} - 1)\,v(t) - (\overline{\mu_1 - \mu_3})\,\overline{\lambda_3}w(t)\\
f_3(t) &= [\overline{\mu_1}(\overline{\lambda_1 - \lambda_2}) - \overline{\lambda_1}(\overline{\mu_1 - \mu_2})]\,u(t) + (\overline{\lambda_1 - \lambda_2})\,v(t) - (\overline{\mu_1 - \mu_2})\,w(t)
\end{aligned}
\tag{A.2}
$$

where

$$
\begin{aligned}
u(t) &= t_y(t)\,s'(t) - (\sigma_{yy}^p + \sigma_{yy}^0)\,x'(t) + (\sigma_{xy}^p + \sigma_{xy}^0)\,y'(t)\\
v(t) &= t_x(t)\,s'(t) - (\sigma_{xy}^p + \sigma_{xy}^0)\,x'(t) + (\sigma_{xx}^p + \sigma_{xx}^0)\,y'(t)\\
w(t) &= t_z(t)\,s'(t) - (\sigma_{yz}^p + \sigma_{yz}^0)\,x'(t) + (\sigma_{xz}^p + \sigma_{xz}^0)\,y'(t).
\end{aligned}
\tag{A.3}
$$

If there is a plane of symmetry normal to the z axis, Eqs. (A.1) and (A.2) reduce to

$$
\begin{aligned}
b_{11} &= \mu_1 - \overline{\mu_2}, \quad & b_{12} &= \mu_2 - \overline{\mu_2}, \quad & b_{13} &= 0\\
b_{21} &= \mu_2 - \overline{\mu_1}, \quad & b_{22} &= \mu_1 - \overline{\mu_1}, \quad & b_{23} &= 0\\
b_{31} &= \overline{\mu_1 - \mu_2}, \quad & b_{32} &= 0, & b_{33} &= 0
\end{aligned}
\tag{A.4}
$$

and

$$
\begin{aligned}
f_1(t) &= -\overline{\mu_2}u(t) - v(t)\\
f_2(t) &= -\overline{\mu_1}u(t) - v(t)\\
f_3(t) &= -(\overline{\mu_1 - \mu_2})\,w(t).
\end{aligned}
\tag{A.5}
$$

Appendix B

The elements of the matrix $[\boldsymbol{Q}]$ in Eq. (25) are

$$
\begin{bmatrix}
l_1^2 & m_1^2 & n_1^2 & 2m_1n_1 & 2n_1l_1 & 2l_1m_1\\
l_2^2 & m_2^2 & n_2^2 & 2m_2n_2 & 2n_2l_2 & 2l_2m_2\\
l_3^2 & m_3^2 & n_3^2 & 2m_3n_3 & 2n_3l_3 & 2l_3m_3\\
l_2l_3 & m_2m_3 & n_2n_3 & m_2n_3 + m_3n_2 & n_2l_3 + n_3l_2 & l_2m_3 + l_3m_2\\
l_3l_1 & m_3m_1 & n_3n_1 & m_1n_3 + m_3n_1 & n_1l_3 + n_3l_1 & l_1m_3 + l_3m_1\\
l_1l_2 & m_1m_2 & n_1n_2 & m_1n_2 + m_2n_1 & n_1l_2 + n_2l_1 & l_1m_2 + l_2m_1
\end{bmatrix}
\tag{B.1}
$$

where l_i, m_i, and n_i are the direction cosines of the n, s, t axes in the global x, y, z coordinate system, i.e.,

$$
\begin{aligned}
l_1 &= \cos(n, x) \quad & m_1 &= \cos(n, y) \quad & n_1 &= \cos(n, z)\\
l_2 &= \cos(s, x) \quad & m_2 &= \cos(s, y) \quad & n_2 &= \cos(s, z)\\
l_3 &= \cos(t, x) \quad & m_3 &= \cos(t, y) \quad & n_3 &= \cos(t, z).
\end{aligned}
\tag{B.2}
$$

By using the dip azimuth β and the dip angle ψ as shown in Fig. 2, Eq. (B.2) can be expressed as

$$
\begin{aligned}
l_1 &= \sin\psi\cos\beta \quad & m_1 &= \cos\psi \quad & n_1 &= \sin\psi\sin\beta\\
l_2 &= -\cos\psi\cos\beta \quad & m_2 &= \sin\psi \quad & n_2 &= -\cos\psi\sin\beta\\
l_3 &= -\sin\beta \quad & m_3 &= 0 \quad & n_3 &= \cos\beta.
\end{aligned}
\tag{B.3}
$$

Acknowledgement

This research is funded in part by National Science Foundation, Grant No. MS-9215397.

References

[1] Ling, C. B.: On the stresses in a notched plate under tension. J. Math. Phys. **26,** 284–289 (1947).
[2] Savage, W. Z., Swolfs, H. S.: Tectonic and gravitational stress in long symmetric ridges and valleys. J. Geophys. Res. **91,** 3677–3685 (1986).
[3] Chiu, C.-H., Gao, H.: Stress singularities along a cycloid rough surface. Int. J. Solids Struct. **30,** 2983–3012 (1993).
[4] Srolovitz, D. J.: On the stability of surfaces of stressed solids. Acta Metall. **37,** 621–625 (1989).
[5] Gao, H.: Stress concentration at slightly undulating surfaces. J. Mech. Phys. Solids **39,** 443–458 (1991).
[6] Gao, H.: Morphological instabilities along surfaces of anisotropic solids. In: Modern theory of anisotropic elasticity and applications (Wu, J. J., Ting, T. C. T., Barnett, D. M., eds.), pp. 139–150. Philadelphia: SIAM 1991.
[7] Pan, E., Amadei, B.: Stresses in an anisotropic rock mass with irregular topography. J. Eng. Mech. **120,** 97–119 (1994).
[8] Amadei, B., Pan, E.: Gravitational stresses in anisotropic rock masses with inclined strata. Int. J. Rock Mech. Min. Sci. Geomech. Abstr. **29,** 225–236 (1992).
[9] Lekhnitskii, S. G.: Theory of elasticity of an anisotropic elastic body. San Francisco: Holden-Day 1963.
[10] Trummer, M. R.: An efficient implementation of a conformal mapping method based on the Szegö kernel. J. Numer. Anal. **23,** 853–872 (1986).
[11] Muskhelishvili, N. I.: Singular integral equations. Groningen: Noordhoff 1972.
[12] Pan, E., Amadei, B., Savage, W. Z.: Gravitational and tectonic stresses in anisotropic rock with irregular topography. Int. J. Rock Mech. Min. Sci. Geomech. Abstr. (under review).
[13] Sarkar, T. K., Yang, X., Arvas, E.: A limited survey of various conjugate gradient methods for solving complex matrix equations arising in electromagnetic wave interactions. Wave Motion **10,** 527–546 (1988).
[14] Amadei, B.: Rock anisotropy and the theory of stress measurements. Berlin Heidelberg New York: Springer 1983.
[15] Lempriere, B. M.: Poisson's ratios in orthotropic materials. J. Am. Inst. Aeronaut. Astronaut. **6,** 2226–2227 (1968).

Authors' address: E. Pan and B. Amadei, University of Colorado, Department of Civil Engineering, Boulder, CO 80309-0428, U.S.A.